HOKKAIDO UNIVERSITY

Title	Catalysis and characterization of carbon-supported ruthenium for cellulose hydrolysis
Author(s)	Komanoya, Tasuku; Kobayashi, Hirokazu; Hara, Kenji et al.
Citation	Applied Catalysis A: General, 407(1-2), 188-194 https://doi.org/10.1016/j.apcata.2011.08.039
Issue Date	2011-11-04
Doc URL	https://hdl.handle.net/2115/47764
Type	journal article
File Information	ACA407-1-2_188-194.pdf

Hokkaido University Collection of Scholarly and Academic Papers : HUSCAP

Catalysis and characterization of carbon-supported ruthenium for cellulose hydrolysis

Tasuku Komanoya [a,b], Hirokazu Kobayashi [a,b], Kenji Hara [a,b], Wang-Jae Chun [c], Atsushi Fukuoka [a,b,*]

[a] Catalysis Research Center, Hokkaido University, Kita 21 Nishi 10, Kita-ku, Sapporo, Hokkaido 001-0021, Japan

[b] Division of Chemical Sciences and Engineering, Graduate School of Chemical Sciences and Engineering, Hokkaido University, Kita 13 Nishi 8, Kita-ku, Sapporo, Hokkaido 060-8628, Japan

[c] Division of Arts and Sciences, International Christian University, 3-10-2 Osawa, Mitaka, Tokyo 181-8585, Japan

* Corresponding Author. Tel.: +81 11 706 9140; Fax: +81 11 706 9139.

E-mail address: fukuoka@cat.hokudai.ac.jp (A. Fukuoka).

Abstract

Ru catalyst supported on mesoporous carbon CMK-3 shows high activity and durability for the hydrolysis of cellulose to glucose in hot compressed water at 503 K. The Ru/CMK-3 catalyst also hydrolyzes cellobiose to glucose in water at 393 K. Several physicochemical methods such as XRD, TEM, XPS, H_2-TPR, O_2-titration, and XAFS were used to characterize active Ru species on CMK-3 and to clarify the formation pathway of the active species. From these studies, we conclude that hydrous Ru oxide $RuO_2 \cdot 2H_2O$ is formed on CMK-3 after H_2-reduction of $RuCl_3$/CMK-3 at 673 K and subsequent passivation at room temperature, and that the Ru oxide nanoparticles with a mean diameter of 1.1 nm are highly dispersed on CMK-3.

Keywords: Biomass, Cellulose, Hydrolysis, Glucose, Supported Ru catalyst, Hydrous ruthenium oxide

1. Introduction

Biomass has been paid significant attention as a renewable carbon resource for fuels and

chemicals [1-3]. The most abundant biomass resource is lignocellulose, produced via photosynthesis using sunlight. In addition, lignocellulose is not digestible for human beings, and its utilization in chemical industry does not compete with food production, which is an advantage of lignocellulose over edible biomass such as sugars and starch. Therefore, lignocellulose is one of the most fascinating biomass resources in nature. Typically, lignocellulose is composed of cellulose, hemicellulose, and lignin, and we have focused on cellulose, accounting for the largest part (40-50%) in those of woods [4].

Cellulose is a polymer of glucose linked by β-1,4-glycosidic bonds [5], and glucose is a potential precursor to useful chemicals such as bioethanol and plastics [6,7]. However, the efficient conversion of cellulose to glucose has been a critical issue, because cellulose shows remarkably low reactivity due to a robust crystal structure with inter- and intra-molecular hydrogen bonds. Therefore, development of effective methods for the hydrolysis of cellulose to glucose is one of the most attractive and challenging subjects in green and sustainable chemistry.

An extensive number of studies have been reported on the hydrolysis of cellulose using mineral acids [8,9] and enzymes [10], but they have drawbacks such as high costs, slow reaction rates, or difficult separation of products and catalysts. Solid acid catalysts have been used to overcome these problems, and several groups reported that supported sulfonic acid catalysts gave good yields of glucose and cello-oligosaccharides in water or ionic liquids [11-17]. However, turnover numbers (TONs) per acid site for the production of glucose were lower than ca. 10, and the sulfonic groups may be leached out in water above 403 K.

In the cellulose conversion by heterogeneous catalysis, we reported the hydrolytic hydrogenation of cellulose to sorbitol by supported metal catalysts [18-20]. Kinetic studies for this reaction indicated that metals promote both hydrolysis and hydrogenation steps [20,21]. Based on these previous works, we found that Ru supported on mesoporous carbon CMK-3 catalyzed the hydrolysis of cellulose to glucose via oligosaccharides (Scheme 1) in hot compressed water even without adding acids [22,23]. In the catalytic reactions, it was suggested that Ru promoted acid-catalyzed reaction, but the catalytic active site has not been elucidated. The purpose of this work is to study the catalytic activity and durability of Ru/CMK-3 in cellulose hydrolysis and to characterize active Ru

species on CMK-3.

Scheme 1

2. Experimental

2.1. Preparation of Ru/CMK-3 catalysts

Mesoporous silica SBA-15 and carbon CMK-3 were synthesized according to the literature methods [24], and the detailed procedures are described in Supporting Information. Ru/CMK-3 catalyst was prepared by a conventional impregnation method using $RuCl_3 \cdot nH_2O$ (99.9%, Wako) as a source of Ru. An aqueous solution of $RuCl_3 \cdot nH_2O$ (5 mL, 53 mg) was added to a mixture of CMK-3 (1.0 g) and distilled water (20 mL). The mixture was stirred for 16 h, and then dried under vacuum for 18 h. The residue was treated with H_2 flow (30 mL min^{-1}) at 673 K for 2 h, and passivated by air or diluted O_2 (10%) in He at room temperature to give 2 wt% Ru/CMK-3. 5 wt% and 10 wt% Ru/CMK-3 catalysts were prepared by a similar method using appropriate amounts of $RuCl_3 \cdot nH_2O$.

2.2. Catalyst characterization

N_2 adsorption-desorption was measured at 77 K ($0.050 \leq p/p_0 \leq 0.995$) using a Belsorp mini II (BEL Japan). Before the measurement, samples were degassed under vacuum (< 10 Pa) at 393 K for 4 h. The N_2 adsorption-desorption isotherms were analyzed by the Brunauer-Emmett-Teller (BET) method to calculate the specific surface area and by the Barrett-Joyner-Halenda (BJH) method to evaluate the pore-size distribution.

Small angle X-ray scattering (SAXS, Rigaku RINT 2000) and powder X-ray diffraction (XRD, Rigaku MiniFlex) were conducted with Cu Kα radiation (0.1542 nm) at an accelerating voltage of 40 kV and a tube current of 40 mA (SAXS) or 30 kV and 15 mA (XRD). The obtained patterns were compared with the references in Joint Committee for Powder Diffraction Standards (JCPDS).

Transmission electron microscopy (TEM) and energy dispersive X-ray spectroscopy (EDS) were performed using a JEM-2100F (JEOL) with an acceleration voltage of 200 kV. Samples were

dispersed on a copper grid with ethanol after ultrasonic pretreatment.

X-ray photoelectron spectroscopy (XPS, JEOL JPC-9010MC) for Ru $3p_{3/2}$ was operated using Al Kα radiation (1486.6 eV) at 100 W and a pass energy of 30 eV. Samples were fixed on a double-stick carbon tape. The binding energies were calibrated using sputtered Au ($4f_{7/2}$ peak at 83.8 eV) [25]. Ru metal (powder, Wako), $RuCl_3 \cdot nH_2O$, RuO_2 (99.95%, Alfa Aesar), and $RuO_2 \cdot nH_2O$ (99.9%, Aldrich) were used as standard compounds, and hereafter the latter is described as $RuO_2 \cdot 2H_2O$, because the water content (n) was estimated to be 2.3 by our thermogravimetric analysis (TGA, Bruker TG-DTA2020S).

H_2-Temperature-programmed reduction (TPR) was performed using a BELCAT (BEL Japan) with 5 vol% of H_2/Ar (30 mL min^{-1}) at a heating rate of 10 K min^{-1} from 323 K to 1273 K. Samples (50 mg) were pretreated with Ar flow (30 mL min^{-1}) at 423 K for 1 h. Outlet gas was analyzed by TCD.

O_2-Titration was measured using the BELCAT with pulses of 5 vol% of O_2/He and He (carrier gas, 30 mL min^{-1}) at 323 K. Before the measurement, samples (50 mg) were reduced with H_2 (30 mL min^{-1}) at 673 K for 2 h, and maintained the temperature at 673 K in He (30 mL min^{-1}) for 15 min to remove the adsorbed H_2. Outlet gas was analyzed by TCD.

Temperature-programmed desorption of pyridine (Pyridine-TPD) was operated with the BELCAT. Samples (50 mg) were preheated with He (30 mL min^{-1}) at 393 K for 30 min, then pyridine-saturated He (vaporized at around 300 K, 30 mL min^{-1}) was introduced onto samples at 393 K for 30 min. After purging the physisorbed pyridine with He (30 mL min^{-1}) at 393 K for 30 min, samples were heated at a heating rate of 10 K min^{-1} from 393 K to 1023 K. Desorbed gasses were analyzed by a mass spectrometer with *m/e* values of 79, 44, and 28 corresponding to pyridine, CO_2, and CO (or N_2), respectively.

Ru K-edge X-ray absorption fine structure (XAFS) measurement was carried out in the transmission mode at 30 K with a He-cryostat using a synchrotron radiation through a Si(331) double-crystal monochromator at NW10A beam line on Photon Factory Advanced Ring (PF-AR; ring energy 6.5 GeV, 450 mA), Institute of Materials Structure Science, High Energy Accelerator Research Organization (KEK), Tsukuba, Japan (Proposal No. 2009G208 and 2010G591). The XAFS

spectra were analyzed using the REX2000 software (Rigaku). Extended X-ray absorption fine structure (EXAFS) spectra were extracted with a spline smoothing method. Fourier transformation of the k^3-weighted EXAFS oscillation was performed in the range of the wave vector k = 3-15 $Å^{-1}$ (Å = 0.1 nm). For the curve-fitting analysis, the backscattering amplitude and the phase shift of Ru–O and Ru–Ru were obtained from RuO_2 and Ru metal.

2.3. Hydrolysis of Cellulose

Cellulose (Merck Avicel, 10 g) was ball-milled to degrade the crystal structure with ZrO_2 balls (1 cm, 1 kg) in a ceramic bottle (900 mL) at 60 rpm for 4 days (96 h) [20,26]. The degree of crystallinity (*CrI*) [27], calculated from the XRD pattern (Figure S1), decreased from 80% (non-treated) to 10% (milled). The water content of cellulose was estimated by a total organic carbon analyzer (TOC, Shimadzu SSM-5000A) to determine the actual weight of the cellulose.

Hydrolysis of cellulose was performed in a hastelloy high-pressure reactor (OM Lab-tech MMJ-100, 100 mL). The ball-milled cellulose (324 mg containing physisorbed water, ca. 2 mmol based on glucose units), catalyst (50 mg), and distilled water (40 mL) were charged into the reactor under air. As a control, He purge to remove air in the reactor did not affect the reaction results. The reactor was heated from 298 to 503 K in 15 min with stirring at 600 rpm by a rotation wing and then immediately cooled by blowing air with continuing the agitation (Figure S2) [28,29]. The pressure in the reactor was increased to 2.8 MPa at 503 K due to the vapor pressure of water.

The reaction mixture was separated to liquid and solid phases by centrifugation and decantation. Products in the solution were analyzed by high-performance liquid chromatography (HPLC, Shimadzu LC10AT*VP*, refractive index detector, typical charts were shown in Figure S3) with a Rezex RPM-Monosaccharide Pb++ (8%) column (ø7.8×300 mm, eluent: water 0.6 mL min^{-1}, 343 K), a Shodex Sugar SH-1011 column (ø8×300 mm, eluent: water 0.5 mL min^{-1}, 323 K), and a TSKgel Amido-80 column (ø4.6×250 mm, eluent: water and acetonitrile (2:3) 0.8 mL min^{-1}, 313 K) to determine the carbon-based yields of water-soluble products by eq 1. The conversion of cellulose was calculated by the weight difference of dried cellulose before and after the reaction (eq 2). The selectivity of product was calculated based on carbon using eq 3.

Yield (%) = (mol of carbon in product) / (mol of carbon in charged cellulose) × 100 (1)

Conversion (%) = {1 – (weight of unreacted cellulose) / (weight of charged cellulose)} × 100 (2)

Selectivity (%) = (yield of product) / (conversion of cellulose) × 100 (3)

The amount of Ru leaching into the liquid phase was checked by inductively coupled plasma atomic emission spectroscopy (ICP-AES, Shimadzu ICPE-9000). The liquid phase was directly analyzed without pretreatment.

3. Results and Discussion

3.1. Catalytic hydrolysis of cellulose

The results of the catalytic hydrolysis of cellulose are summarized in Table 1. In a blank test without catalyst (entry 1), the conversion of cellulose was 24% and small amounts of glucose (4.6%) and cello-oligosaccharides (14%, dimer to octamer) formed with other minor by-products such as fructose and 5-hydroxymethylfurfural, thereby showing that hot compressed water can hydrolyzes cellulose by the ionic products (H_3O^+ and OH^-) or by the direct attack of water molecules as the precedent work reported [30]. It is noticeable that CMK-3 significantly increased the conversion of cellulose (54%) and the yields of glucose (16%) and oligomers (22%) (entry 3), and the selectivity for the sum of glucose and oligomers was 71%. This promotion of cellulose hydrolysis might be ascribed to acidic oxygenated-functional groups on CMK-3 (410 μmol g^{-1}, determined by NaOH titration), which can adsorb β-glucans [13]. Over the Ru/CMK-3 catalysts, the yield of glucose increased to 24% (Ru 2 wt%, entry 4), 26% (Ru 5 wt%, entry 6), and 31% (Ru 10 wt%, entry 7), and the increases by Ru are 8%, 10%, and 15%, respectively, by subtracting the yield with CMK-3 (16%). 2 wt% Ru on CMK-3 gave the maximum TON (= 15) for the production of glucose (150 μmol) based on bulk Ru (10 μg-atom). The TON is comparable to those of previously reported solid sulfonic acid catalysts (TONs based on SO_3H < 12) [11-17]. However, the total reaction time including cooling to room temperature (50 min, Figure S2) is shorter than those of the sulfonic acid systems (typically 24 h), and the turnover frequency (TOF) of Ru (18 h^{-1}) is significantly higher than

the maximum TOF of SO_3H (0.5 h^{-1}). In addition, we tested a reaction maintaining the temperature at 463 K for 2 h (entries 2 and 5). Although this reaction with 2 wt% Ru/CMK-3 gave glucose in 20% yield (entry 5), the oligomer yield was significantly depressed and the 5-HMF yield was slightly enhanced compared to those of entry 4. It is thus shown that the rapid heating-cooling method is more favorable to obtain high selectivity for glucose and oligomers.

Table 1

In contrast to the increase of glucose yield by increasing the Ru loading, the yield of oligomers decreased from 22% to 5%, but interestingly the total yields of glucose and oligomers were kept constant at ca. 40% in these reactions. With increase of Ru loading, the selectivity for glucose and oligomers lowered (71% to 55%) due to the increase of the cellulose conversion (54% to 68%). This trade-off between selectivity and conversion is a character of the high reactivity of glucose, thus showing that formation and decomposition of glucose occur simultaneously during the reactions. In fact, decomposition of glucose (40%) was observed under the same reaction conditions without catalysts. Thereby, the total yield of glucose and oligomers leveled off at 40% despite the increase of cellulose conversion. Based on the above discussion, we propose the roles of CMK-3 and Ru species as follows: (1) CMK-3 converts cellulose to oligomers and glucose along with the effect of hot compressed water (entry 1 to 3). (2) Ru is more effective to increase the glucose yield than CMK-3 (entries 3 and 4). This synergy enables the efficient hydrolysis of cellulose to glucose. We also performed the screening of supports (Table S1) and metals (Table S2), in which 2 wt% Ru/CMK-3 gave the highest TON of metal for glucose formation. Accordingly, 2 wt% Ru/CMK-3 catalyst was chosen for further studies.

To check the hydrolytic activities of Ru for the depolymerization of oligomers, the hydrolysis of cellobiose was performed as a test reaction. The reactions were carried out at a temperature as low as 393 K for 24 h to minimize the hydrolysis by hot compressed water and to avoid the further decomposition of glucose as observed at 503 K (Scheme 2). As shown in Table 2, CMK-3 did not show clear catalytic activity under the mild reaction conditions (entry 9). On the contrary, 2 wt%

Ru/CMK-3 improved the glucose yield to 23% (entry 10). It is thus suggested that the Ru species on CMK-3 works as an acid catalyst to hydrolyze β-1,4-glycosidic bonds of oligomers to yield glucose.

Scheme 2

Table 2

The durability of catalysts is an important factor for the practical application. From this viewpoint, the reuse experiments of 2 wt% Ru/CMK-3 catalyst were performed, and the results are summarized in Figure 1. The solid phase containing the catalyst and unreacted cellulose in the preceding reaction was recovered from the reaction mixture by centrifugation. The solid was directly used for the next reaction without pretreatment by adding fresh cellulose of 324 mg, and the yields were calculated based on the added fresh cellulose. The yields of glucose were in the range of 20-21% in these experiments. Although the yield of oligomers increased in the first three runs as the remaining cellulose in the previous reactions was hydrolyzed, steady results were obtained after the 3rd run. As the conversion of cellulose is ca. 50% in the first reaction, the influence of unreacted cellulose increases in the first three runs by considering the geometric sequence of the accumulation, but becomes almost constant after the 3rd run. Furthermore, remaining cellulose in the previous reactions shows lower reactivity than fresh one because of the transformation of amorphous cellulose to cellulose IV crystal (detected by XRD, not shown). Therefore, the steady results with the good yield of glucose from the 3rd run indicate that the catalytic activity is stable at least after the 3rd run. ICP-AES measurement of the liquid phase after the reaction showed no Ru leaching (less than 0.2 mol%). Furthermore, the use of water solvent filtrated after heating with Ru/CMK-3 catalyst at 503 K did not promote the hydrolysis of cellulose without catalyst (glucose 3.6%, oligomers 15%, conv. 27%) in accord with the control experiment using pure water (glucose 4.6%, oligomers 14%, conv. 24%, Table 1 entry 1). Therefore, Ru/CMK-3 catalyst is reusable for the hydrolysis of cellulose by easy separation.

Figure 1

3.2. Characterization of Ru/CMK-3 catalyst

Several physicochemical methods were used for the characterization of Ru/CMK-3. N_2 adsorption-desorption was performed for CMK-3, Ru/CMK-3, and Ru/CMK-3-W treated in hot compressed water at 503 K. The three samples exhibited almost identical type IV isotherms (Figure S4) [31] and textural properties (Table S3). The SAXS data also verified the ordered mesoporous structure for the samples (Figure 2a). These results indicate that the ordered mesopores are stable in the impregnation of Ru and in the treatment in water at 503 K.

Figure 2

In the XRD measurement (Figure 2b), CMK-3 showed two broad peaks at 23° and 43° due to the turbostratic carbon. Ru/CMK-3 and Ru/CMK-3-W provided no diffraction peaks of Ru, indicating the absence of large Ru crystals. TEM images of Ru/CMK-3 show the ordered mesoporous structure of CMK-3 (Figure 3a) and dark dots of well-dispersed particles with a mean diameter of 1.1 nm (Figure 3b,c). The EDS spectrum of Ru/CMK-3 indicated the presence of Ru for Ru/CMK-3 (Figure S5). From these results, the particles observed in TEM (Figure 3b) are assignable to a certain type of Ru nanoparticles, and the possible reasons for no diffraction peak of Ru metal in XRD are as follows: (1) metallic Ru crystals are too small to give diffraction peaks in XRD or (2) Ru is not in zero-valent.

Figure 3

It is known that the surface of Ru metal is easily oxidized by O_2 even at room temperature [32]. In our experiments, Ru/CMK-3 was gently passivated in diluted O_2 at room temperature after the H_2-reduction at 673 K in the catalyst preparation. If the oxidation state of Ru is higher than zero, the Ru species may give an acidic site as discussed in the literature [33]. To characterize the Ru species on CMK-3, XPS was conducted for Ru/CMK-3, in which the Ru loading was increased to 10 wt% to

gain a good S/N ratio (Figure S6). Ru metal, $RuCl_3$, RuO_2, and $RuO_2 \cdot 2H_2O$ were also used as reference materials. In this XPS analysis, the binding energy of Ru $3p_{3/2}$ orbital was measured, because the peak of Ru $3d_{5/2}$ was overlapped with that of C 1s [34]. As shown in Figure S6, the binding energy of Ru/CMK-3 (461.9 eV) was higher than that of Ru metal (460.7 eV), but similar to those of $RuCl_3$ (462.1 eV), RuO_2 (461.5 eV), $RuO_2 \cdot 2H_2O$ (461.9 eV), and Ru/CMK-3-A (461.7 eV) which was the spent catalyst used for the cellulose hydrolysis at 503 K. It is thus indicated that the Ru species on CMK-3 is not in zero-valent but in tri- or tetra-valent state.

To clarify the formation mechanism for the cationic Ru on CMK-3, two types of titration experiments were performed. Firstly, the H_2-TPR experiments were conducted for $RuCl_3$ supported on CMK-3 (denoted as $RuCl_3$/CMK-3, Ru loading 2 wt%) (Figure 4). The TPR profile of $RuCl_3$/CMK-3 shows two major peaks at 400 K and 800 K; the peak at 400 K results from the reduction of $RuCl_3$ and the latter at 800 K is ascribed to the methanation of CMK-3 by comparing with the profile of CMK-3 [35]. The H/Ru uptake for the reduction was calculated to be 4.2, which was higher than 3 for the stoichiometric reduction of $RuCl_3$ ($RuCl_3 + 3/2\ H_2 \rightarrow Ru + 3\ HCl$). The excess H_2 might be used for the reduction of surface functional groups such as quinones on CMK-3 [35], because the H/Ru value was decreased with increase in the Ru loading: 3.3 for 5 wt% and 2.9 for 10 wt% (Figure S7). Accordingly, we conclude that $RuCl_3$ on CMK-3 is completely reduced to Ru metal during the H_2-reduction at 673 K (Scheme 3).

Figure 4

Scheme 3

Secondly, the O_2-pulse titration experiments were performed in situ after the H_2-reduction at 673 K. The O/Ru uptake was 1.8, indicating that Ru metal on CMK-3 was almost completely oxidized to RuO_2 (Scheme 3). On the other hand, Ru particles (crystalline size 25 nm by XRD) prepared by the reduction of $RuCl_3$ without supporting onto CMK-3 showed diffraction peaks of crystalline Ru after the passivation treatment (Figure S8). Therefore, the carbon support CMK-3 gives highly dispersed Ru nanoparticles after H_2-reduction at 673 K, but the resulting Ru nanoparticles are so small and

reactive to O_2 in air or He at room temperature to give RuO_2 nanoparticles (1.1 nm) observed in TEM (Figure 3b). Hence the role of H_2 pretreatment is to produce the reactive Ru nanoparticles which are the precursor to RuO_2 species with removing Cl.

Ru K-edge XAFS was performed for further characterization of the Ru species on CMK-3. In normalized XANES spectra (Figure 5), the absorption edges are corrected based on that of Ru metal (22117 eV) [36]. It is found that the edge energy of Ru/CMK-3 (22127 eV) is the same as those of $RuO_2 \cdot 2H_2O$ and RuO_2. The shape of spectrum for Ru/CMK-3 is also similar to those of RuO_2 and $RuO_2 \cdot 2H_2O$, whereas $RuCl_3$ and Ru metal give distinctly different spectra. The spectrum of Ru/CMK-3-A shows a small difference from that of fresh Ru/CMK-3 catalyst (Figure S9). Mo et al. reported analogous slight change of XANES spectra in the electrochemical reduction of Ru(IV) to Ru(III) for hydrous RuO_x films [37]. Accordingly, we propose that Ru(IV) is partially reduced to Ru(III) after the catalytic reaction. By the curve-fitting of the spectrum of Ru/CMK-3-A with those of $RuCl_3$ and $RuO_2 \cdot 2H_2O$, the Ru(III)/Ru(IV) ratio is estimated to be 2/3. One possible reducing agent is glucose produced in the catalytic reaction.

Figure 5

EXAFS oscillations for Ru/CMK-3 and reference materials are shown in Figure S10. The EXAFS oscillation of Ru/CMK-3 resembles that of $RuO_2 \cdot 2H_2O$, but apparently differs from those of RuO_2, $RuCl_3$, and Ru metal (Figure S10a). As discussed above, the O_2-titration indicates that RuO_2 is formed on CMK-3 by passivation, and the above result suggests that RuO_2 adsorbs two H_2O molecules from moisture in air to give $RuO_2 \cdot 2H_2O$ on CMK-3. In addition, different oscillations of Ru/CMK-3 and Ru/CMK-3-A were observed above 7 Å (Figure S10b). This may be due to the reduction of Ru(IV) to Ru(III) for RuCMK-3-A, which was suggested by XANES (vide supra).

Fourier transforms of the EXAFS spectra for Ru/CMK-3, $RuO_2 \cdot 2H_2O$, and RuO_2 are depicted in Figure 6. It is clearly shown that Ru/CMK-3 and $RuO_2 \cdot 2H_2O$ provide similar curves, giving two strong peaks at ca. 1.5 Å and 2.6 Å assigned to Ru–O and Ru–(O)–Ru shells, respectively [38]. Besides the two peaks, RuO_2 has a characteristic peak at 3.2 Å due to another Ru–(O)–Ru shell in

the rutile structure [38,39]. For Ru/CMK-3-A (Figure S11), a strong peak at 1.5 Å is due to Ru–O, and a peak at 2.4 Å is assignable to another type of Ru–Ru shell (vide infra).

Figure 6

Based on the assignment for the peaks, curve-fitting analysis of the EXAFS oscillations were performed, and the results are summarized in Table 3. Figure 7 shows proposed structures of the Ru catalysts. It is worth noting that Ru/CMK-3 gives almost the same results as those of $RuO_2 \cdot 2H_2O$ for Ru–O and Ru–Ru shells. McKeown et al. proposed that $RuO_2 \cdot 2H_2O$ takes a one-dimensional chain structure (Figure 7c) because of the presence of Ru–O (2.0 Å) and short Ru–Ru (3.1 Å) shells and the absence of long Ru–Ru (3.54 Å) shell as observed for RuO_2 [38]. Therefore, we propose that Ru/CMK-3 has a one-dimensional structure like $RuO_2 \cdot 2H_2O$ as depicted in Figure 7a. Lack of the Ru–O shell at ca. 3.5 Å, which is observed for RuO_2, also supports the one-dimensional structure for Ru/CMK-3.

Figure 7

By considering the mean diameter of nanoparticles (1.1 nm) in TEM (Figure 3), Figure 7a shows a proposed structure in accord with this size. In this structure, Ru is surrounded by six O atoms in a distance of 1.98 Å, where four O atoms are bridging to Ru (Ru–O–Ru) and the Ru–Ru distance is 3.06 Å. Other two O atoms are suggested to be derived from coordinated H_2O, thereby fulfilling the atomic stoichiometry and the valence state of $RuO_2 \cdot 2H_2O$. In addition, Ru/CMK-3 and $RuO_2 \cdot 2H_2O$ have small peaks at 2.1 Å in the Fourier transforms (Figure 6), which might be due to another Ru–O shell from hydrogen-bonded H_2O molecules on the bridging O atoms [37].

The spent catalyst Ru/CMK-3-A has a slightly longer Ru–O distance (2.04 Å) than Ru/CMK-3 (1.98 Å), which is similar to that of $[Ru(H_2O)_6]^{3+}$ (2.03 Å) [38]. This result also indicates the presence of Ru(III) species in Ru/CMK-3-A. For the Ru–Ru shell, Ru/CMK-3-A has a shorter distance of 2.93 Å than Ru/CMK-3 (3.06 Å), and this shrinkage may correspond to the decrease of

the electrostatic repulsion by the partial change of Ru(IV) to Ru(III) in the one-dimensional structure of the hydrous RuO_2.

From these results, it is concluded that Ru/CMK-3 has highly dispersed $RuO_2 \cdot 2H_2O$ on CMK-3 as represented in Figure 7a.

3.3. Role of Ru in cellulose hydrolysis

As discussed in section 3.1, the hydrolysis of cellulose and oligomers are promoted under the hot compressed water by H_3O^+ from the dissociation of water or by the direct attack of H_2O [30], CMK-3, and the Ru species on CMK-3. In the model experiments using cellobiose, the Ru species showed promotional effect for the hydrolysis of β-1,4-glycosidic bonds. Hence, we focus on the role of Ru in the cellulose hydrolysis. By the several physicochemical analyses, the Ru species is identified to $RuO_2 \cdot 2H_2O$ (Figure 7a). As to the acidic property, Ru/CMK-3-dispersed water is neutral (pH 6.3 at 298 K), thus indicating that the Ru species is not a homogeneous acid catalyst. It is known that $[Ru(H_2O)_6]^{3+}$ produces H^+ and $[Ru(H_2O)_5OH]^{2+}$ (pK_a = 2.9 at 298 K) [40], implying that $RuO_2 \cdot 2H_2O$ may give a Brønsted acid by the similar mechanism, because the cellulose hydrolysis is performed in water media. On the other hand, it was proposed that a Ru(III) phosphotungstate catalyzes the hydrolysis of cellulose as a Lewis acid [33]. In our case, the dissociation of a water molecule coordinated on Ru could give a vacant site with Lewis acidity.

To investigate the acid sites on Ru, we tried to measure FT-IR spectra of pyridine adsorbed on Ru/CMK-3, but no peaks of adsorbed pyridine were observed. We also performed pyridine-TPD experiments using 2 wt% Ru/CMK-3 and CMK-3. In Figure S12, the peaks at 500 K are attributed to pyridine desorbed from weak acid sites like COOH on CMK-3 [41]. On 2 wt% Ru/CMK-3, the peaks of CO (or N_2) and CO_2 were observed by the decomposition of pyridine on Ru [42,43], but no specific peaks due to acid sites were observed by comparing the results of CMK-3. Presumably, the acid site is formed under the reaction conditions in the hot compressed water. The origin of acidity is now under study.

4. Conclusion

Ru/CMK-3 catalyst shows good activity and durability for the hydrolysis of cellulose to glucose in hot compressed water at 503 K without additional acids. The Ru/CMK-3 catalyst also hydrolyzes cellobiose into glucose even at 393 K. By detailed characterization of Ru/CMK-3 using several physicochemical methods, it is demonstrated that the catalytic active species is $RuO_2 \cdot 2H_2O$ formed by the reduction and passivation of $RuCl_3$ on CMK-3. Highly dispersed Ru nanoparticles are formed from $RuCl_3$ on CMK-3 by the H_2-reduction at 673 K, and the Ru particles are quantitatively oxidized to RuO_2 during the passivation at room temperature. Finally, RuO_2 adsorbs moisture in air to form highly dispersed $RuO_2 \cdot 2H_2O$ particles with the one-dimensional chain structure. It is also indicated that a part of Ru(IV) species on CMK-3 is reduced to Ru(III) after the catalytic reaction, but the structure still maintains to give good durability of this catalyst. Accordingly, we conclude that the hydrous ruthenium oxide on CMK-3 is a water-tolerant solid catalyst for the production of glucose from cellulose.

Acknowledgment

The authors thank Prof. K. Asakura for helpful discussions about XAFS analyses. This work was supported by a Grant-in-Aid for Scientific Research (KAKENHI, 20226016) from the Japan Society for the Promotion of Science (JSPS). T. Komanoya appreciates the JSPS Research Fellowship for Young Scientists.

Appendix A. Supplementary data

Supplementary data associated with this article can be found, in the online version, at doi:

References

[1] J.N. Chheda, G.W. Huber, J.A. Dumesic, Angew. Chem. Int. Ed. 46 (2007) 7164-7183.

[2] T.-M. Hsin, S. Chen, E. Guo, C.-H. Tsai, M. Pruski, V. S.-Y. Lin, Top. Catal. 53 (2010) 746-754.

[3] D. Klemm, B. Heublein, H.-P. Fink, A. Bohn, Angew. Chem. Int. Ed. 44 (2005) 3358-3393.

[4] Y. Sun, J. Cheng, Bioresour. Technol. 83 (2002) 1-11.

[5] S.K. Guha, H. Kobayashi, A. Fukuoka, in: M. Crocker (Ed.), Thermochemical Conversion of

Biomass to Liquid Fuels and Chemicals, RSC Publishing, Cambridge, 2010, pp. 344.

[6] P.L. Dhepe, A. Fukuoka, ChemSusChem 1 (2008) 969-975.

[7] J.J. Bozell, G.R. Petersen, Green Chem. 12 (2010) 539-554.

[8] R. Rinaldi, F. Schüth, ChemSusChem 2 (2009) 1096-1107.

[9] M.A. Harmer, A. Fan, A. Liauw, R.K. Kumar, Chem. Commun. (2009) 6610-6612.

[10] K.H. Kim, J. Hong, Bioresour. Technol. 77 (2001) 139-144.

[11] S. Suganuma, K. Nakajima, M. Kitano, D. Yamaguchi, H. Kato, S. Hayashi, M. Hara, J. Am. Chem. Soc. 130 (2008) 12787-12793.

[12] D. Yamaguchi, M. Kitano, S. Suganuma, K. Nakajima, H. Kato, M. Hara, J. Phys. Chem. C 113 (2009) 3181-3188.

[13] M. Kitano, D. Yamaguchi, S. Suganuma, K. Nakajima, H. Kato, S. Hayashi, M. Hara, Langmuir 25 (2009) 5068-5075.

[14] A. Onda, T. Ochi, K. Yanagisawa, Green Chem. 10 (2008) 1033-1037.

[15] R. Rinaldi, R. Palkovits, F. Schüth, Angew. Chem. Int. Ed. 47 (2008) 8047-8050.

[16] S. Van de Vyver, L. Peng, J. Geboers, H. Schepers, F. de Clippel, C.J. Gommes, B. Goderis, P.A. Jacobs, B.F. Sels, Green Chem. 12 (2010) 1560-1563.

[17] J. Pang, A. Wang, M. Zheng, T. Zhang, Chem. Commun. 46 (2010) 6935-6937.

[18] A. Fukuoka, P.L. Dhepe, Angew. Chem. Int. Ed. 45 (2006) 5161-5163.

[19] H. Kobayashi, H. Matsuhashi, T. Komanoya, K. Hara, A. Fukuoka, Chem. Commun. 47 (2011) 2366-2368.

[20] H. Kobayashi, Y. Ito, T. Komanoya, Y. Hosaka, P. L. Dhepe, K. Kasai, K. Hara, A. Fukuoka, Green Chem. 13 (2011) 326-333.

[21] V. Jollet, F. Chambon, F. Rataboul, A. Cabiac, C. Pinel, E. Guillon, N. Essayem, Green Chem. 11 (2009) 2052-2060.

[22] H. Kobayashi, T. Komanoya, K. Hara, A. Fukuoka, ChemSusChem 3 (2010) 440-443.

[23] K. Matsumoto, H. Kobayashi, K. Ikeda, T. Komanoya, A. Fukuoka, S. Taguchi, Bioresour. Technol. 102 (2011) 3564-3567.

[24] S. Jun, S.H. Joo, R. Ryoo, M. Kruk, M. Jaroniec, Z. Liu, T. Ohsuna, O. Terasaki, J. Am. Chem.

Soc. 122 (2000) 10712-10713.

[25] N. Ikeo, Y. Iijima, N. Nimura, M. Sigematsu, T. Tazawa, S. Matsumoto, K. Kojima, Y. Nagasawa, Handbook of X-ray Photoelectron Spectroscopy, JEOL, Tokyo, 1991.

[26] H. Zhao, J.H. Kwak, Y. Wang J.A. Franz, J.M. White, J.E. Holladay, Energy Fuels 20 (2006) 807.

[27] Y.-H.P. Zhang, L.R. Lynd, Biotechnol. Bioeng. 10 (2004) 797-824.

[28] T. Minowa, F. Zhen, T. Ogi, J. Supercrit. Fluids 13 (1998) 253-259.

[29] T. Minowa, T. Ogi, Catal. Today 45 (1998) 411-416.

[30] O. Bobleter, Prog. Polym. Sci. 19 (1994) 797-841.

[31] K.S.W. Sing, D.H. Everett, R.A.W. Haul, L. Moscou, R.A. Pierotti, J. Rouquerol, T. Siemieniewska, Pure Appl. Chem. 57 (1985) 603-619.

[32] P.G.J. Koopman, A.P.G. Kieboom, H. van Bekkum, J. Catal. 69 (1981) 172-179.

[33] K. Shimizu, H. Furukawa, N. Kobayashi, Y. Itaya, A. Satsuma, Green Chem. 11 (2009) 1627-1632.

[34] J. Ren, J. Ding, K.-Y. Chan, H. Wang, Chem. Mater. 19 (2007) 2786-2795.

[35] X. Yang, X. Wang, J. Qiu, Appl. Catal. A: Gen. 382 (2010) 131-137.

[36] R. Viswanathan, G. Hou, R. Liu, S.R. Bare, F. Modica, G. Mickelson, C.U. Segre, N. Leyarovska, E.S. Smotkin, J. Phys. Chem. B 106 (2002) 3458-3465.

[37] Y. Mo, M.R. Antonio, D.A. Scherson, J. Phys. Chem. B 104 (2000) 9777-9779.

[38] D.A. McKeown, P.L. Hagans, L.P.L. Carette, A.E. Russell, K.E. Swider, D.R.J. Rolison, Phys. Chem. B 103 (1999) 4825-4832.

[39] T. Arikawa, Y. Takasu, Y. Murakami, K. Asakura, Y. Iwasawa, J. Phys. Chem. B 102 (1998) 3736-3741.

[40] W. Böttcher, G.M. Brown, N. Sutin, Inorg. Chem. 18 (1979) 1447-1451.

[41] J.M. Campelo, A. Garcia, D. Luna, J.M. Marinas, A.A. Romero, Thermochim. Acta 261 (1995) 175-182.

[42] R.W. Stevens Jr., S.S.C. Chuang, B.H. Davis, Appl. Catal. A: Gen. 252 (2003) 57-74.

[43] J.L. Figueiredo, M.F.R. Pereira, M.M.A. Freitas, J.J.M. Órfão, Carbon 37 (1999) 1379–1389.

Table 1. Hydrolysis of Cellulose by CMK-3 and Ru/CMK-3 Catalysts[a].

entry	Catalyst	yield based on carbon (%)							total yield (%)	conv (%)[b]
		glucose	oligomers[c]	fructose	mannose	levoglucosan	5-HMF[d]	furfural		
1	Blank	4.6 (19)	14.1 (58)[e]	0.9	0.6	0.1	1.8	0.4	22.6	24.2
2[h]	Blank	4.9 (22)	4.9 (22)	0.9	0.5	0.5	4.8	0.8	17.3	22.5
3	CMK-3	15.9 (30)	22.1 (41)[f]	2.0	1.4	1.1	4.3	0.6	47.3	53.6
4	2 wt% Ru/CMK-3	23.8 (43)	16.2 (29)[g]	1.7	1.3	1.8	2.8	0.4	48.0	55.9
5[h]	2 wt% Ru/CMK-3	20.4 (43)	3.0 (6)	1.9	1.0	0.9	7.1	0.7	35.1	47.5
6	5 wt% Ru/CMK-3	25.9 (42)	10.3 (17)	1.9	1.0	1.7	2.7	0.2	43.7	62.2
7	10 wt% Ru/CMK-3	31.2 (47)	5.1 (8)	1.9	1.1	2.4	1.9	0.3	41.8	67.6

[a] Cellulose 324 mg (2 mmol, 50 mM based on glucose unit), catalyst 50 mg, water 40 mL, 503 K, < 1 min. Selectivity based on the conversion of cellulose is shown in parentheses. [b] Cellulose conversion is calculated from the weight decrease of the solid during the reaction. [c] Dimer-octamer. [d] 5-Hydroxymethylfurfural. [e] Dimer 3.0%, trimer 3.4%, tetramer 3.2%, pentamer 1.7%, hexamer 1.6%, heptamer < 1%. [f] Dimer 8.4%, trimer 6.9%, tetramer 4.2%, pentamer 2.0%, hexamer < 1%. [g] Dimer 8.3%, trimer 4.8%, tetramer 2.3%, pentamer < 1%. [h] 463 K, 2 h.

Table 2. Hydrolysis of Cellobiose by Ru/CMK-3 Catalyst at 393 K[a].

entry	Catalyst	glucose	mannose	fructose	5-HMF	total (%)
8	Blank	5.7	0.0	0.0	1.0	6.7
9	CMK-3	4.7	0.0	0.2	0.0	4.9
10	2 wt% Ru/CMK-3	22.5	1.1	0.2	0.1	23.8

[a] Cellobiose 342 mg (2 mmol, 50 mM based on glucose unit), catalyst 50 mg, water 40 mL, 393 K, 24 h.

Table 3. Curve-fittings of 2 wt% Ru/CMK-3, the Spent Catalyst Ru/CMK-3-A, $RuO_2 \cdot 2H_2O$, and RuO_2.

sample	shell	CN[a]	R (Å)[b]	σ^2 (Å^2)[c]	ΔE_0 (eV)[d]	R_f (%)[e]
Ru/CMK-3	Ru–O	6.9 ± 1.4	1.98 ± 0.02	0.0137 ± 0.0004	0.0 ± 3.3	9.7
	Ru–Ru	1.0 ± 0.4	3.06 ± 0.02	0.0067 ± 0.0005	-1.1 ± 3.6	
Ru/CMK-3-A	Ru–O	7.9 ± 1.8	2.04 ± 0.02	0.0132 ± 0.0005	6.6 ± 3.4	4.3
	Ru–Ru	1.6 ± 0.6	2.93 ± 0.02	0.0100 ± 0.0005	-10.4 ± 3.8	
$RuO_2 \cdot 2H_2O$	Ru–O	6.4 ± 1.3	2.01 ± 0.02	0.0090 ± 0.0004	4.6 ± 3.2	12.9
	Ru–Ru	1.4 ± 0.4	3.10 ± 0.01	0.0046 ± 0.0004	7.7 ± 2.8	
RuO_2	Ru–O	6[f]	1.97[f,g]	0.0034 ± 0.0004	-0.1 ± 2.8	1.7
	Ru–Ru	2[f]	3.11[f]	0.0035 ± 0.0003	-1.1 ±2.9	
	Ru–Ru	8[f]	3.54[f]	0.0035 ± 0.0000	-0.2 ± 1.0	

[a] Average coordination number. [b] Interatomic distance. [c] Debye-Waller factor. [d] Edge shift. [e] R factor. [f] Fixed at the values from the crystallographic data. [g] Average value.

Figure captions

Figure 1. Reuse experiments of 2 wt% Ru/CMK-3 catalyst for the cellulose hydrolysis at 503 K. "Oligomers" bar is the total yield of dimer-octamer, and "By-products" bar is that of fructose, mannose, levoglucosan, 5-hydroxymethylfurfural, and furfural.

Figure 2. (a) SAXS and (b) XRD patterns of CMK-3, 2 wt% Ru/CMK-3, and Ru/CMK-3-W treated in water at 503 K.

Figure 3. (a, b) TEM images of 2 wt% Ru/CMK-3 and (c) particle size distribution of the Ru species.

Figure 4. H_2-TPR profiles of 2 wt% $RuCl_3$/CMK-3 and CMK-3.

Figure 5. Ru K-edge XANES spectra of (i) 2 wt% Ru/CMK-3, (ii) 2 wt% Ru/CMK-3-A, (iii) $RuO_2 \cdot 2H_2O$, (iv) RuO_2, (v) $RuCl_3$, and (vi) Ru metal.

Figure 6. Fourier transforms of k^3-weighted Ru K-edge EXAFS spectra for (i) 2 wt% Ru/CMK-3, (ii) 2 wt% Ru/CMK-3-A, (iii) $RuO_2 \cdot 2H_2O$, (iv) RuO_2 (x 1/3 intensity), (v) $RuCl_3$ (x 1/3), and (vi) Ru metal (x 1/15). Figure 7. Proposed structures of (a) Ru/CMK-3 and (b) Ru/CMK-3-A and referenced structures of (c) $RuO_2 \cdot 2H_2O$ and (d) RuO_2.

Scheme 1. Hydrolysis of cellulose to glucose by Ru/CMK-3 catalyst.

Scheme 2. Hydrolysis of cellobiose to glucose.

Scheme 3. Formation pathway of the oxidized Ru species on CMK-3 during the catalyst preparation.

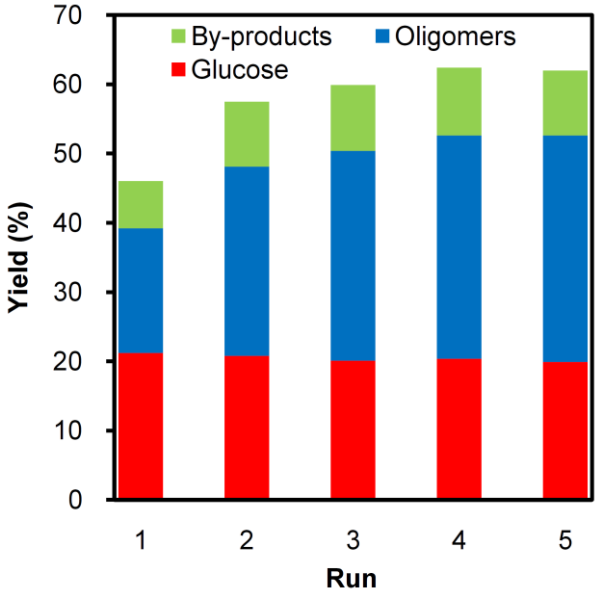

Figure 1. Reuse experiments of 2 wt% Ru/CMK-3 catalyst for the cellulose hydrolysis at 503 K. "Oligomers" bar is the total yield of dimer-octamer, and "By-products" bar is that of fructose, mannose, levoglucosan, 5-hydroxymethylfurfural, and furfural.

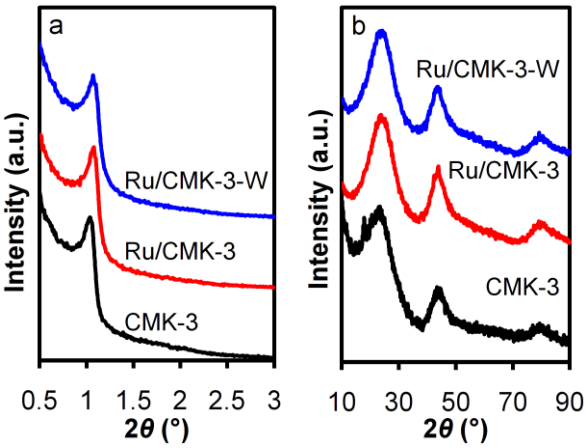

Figure 2. (a) SAXS and (b) XRD patterns of CMK-3, 2 wt% Ru/CMK-3, and Ru/CMK-3-W treated in water at 503 K.

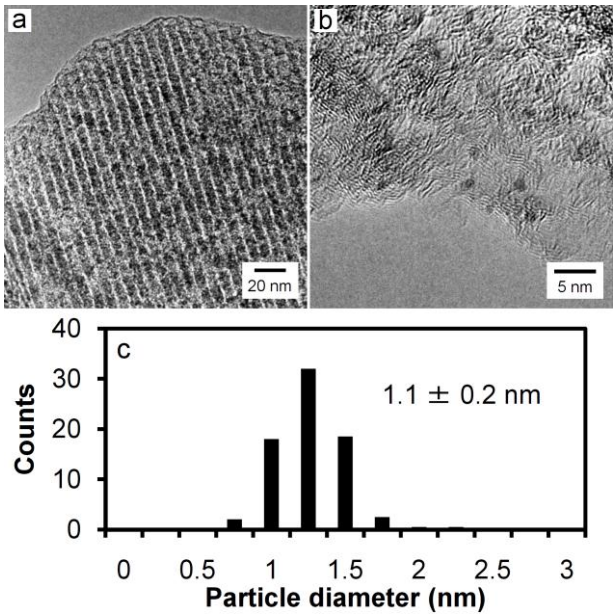

Figure 3. (a, b) TEM images of 2 wt% Ru/CMK-3 and (c) particle size distribution of the Ru species.

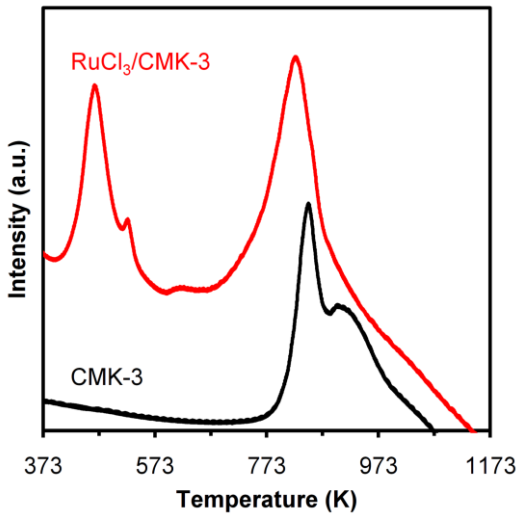

Figure 4. H_2-TPR profiles of 2 wt% $RuCl_3$/CMK-3 and CMK-3.

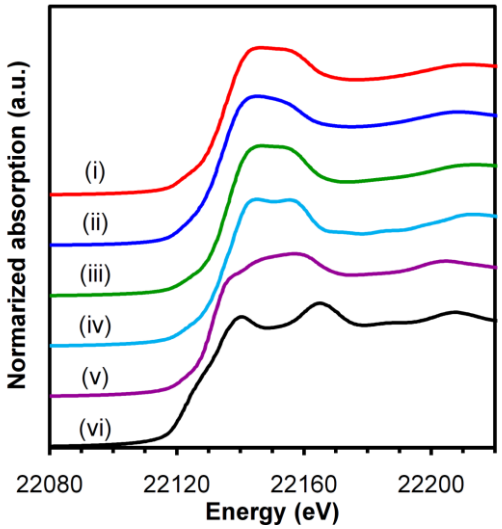

Figure 5. Ru K-edge XANES spectra of (i) 2 wt% Ru/CMK-3, (ii) 2 wt% Ru/CMK-3-A, (iii) $RuO_2 \cdot 2H_2O$, (iv) RuO_2, (v) $RuCl_3$, and (vi) Ru metal.

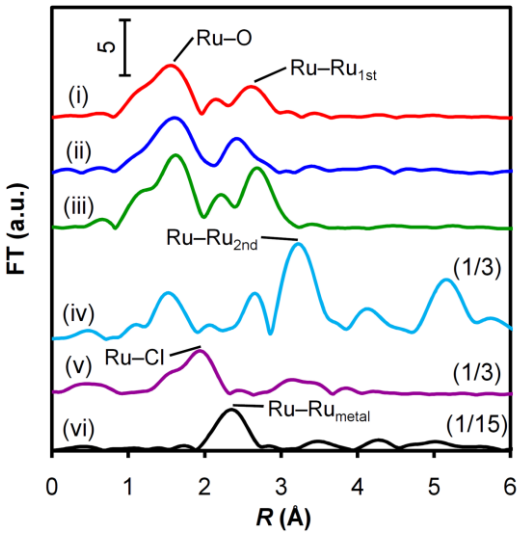

Figure 6. Fourier transforms of k^3-weighted Ru K-edge EXAFS spectra for (i) 2 wt% Ru/CMK-3, (ii) 2 wt% Ru/CMK-3-A, (iii) $RuO_2 \cdot 2H_2O$, (iv) RuO_2 (x 1/3 intensity), (v) $RuCl_3$ (x 1/3), and (vi) Ru metal (x 1/15).

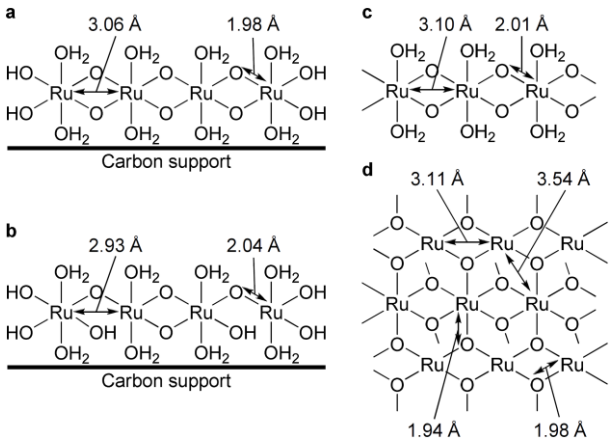

Figure 7. Proposed structures of (a) Ru/CMK-3 and (b) Ru/CMK-3-A and referenced structures of (c) $RuO_2 \cdot 2H_2O$ and (d) RuO_2.

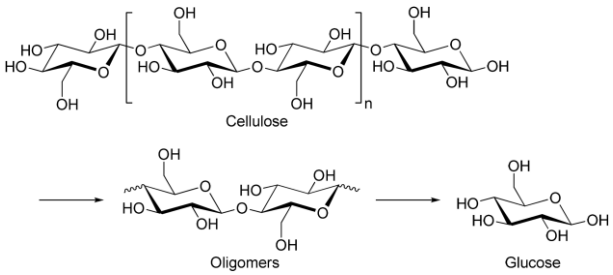

Scheme 1. Hydrolysis of cellulose to glucose by Ru/CMK-3 catalyst.

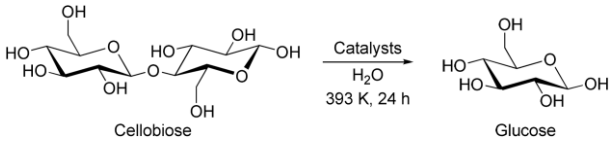

Scheme 2. Hydrolysis of cellobiose to glucose.

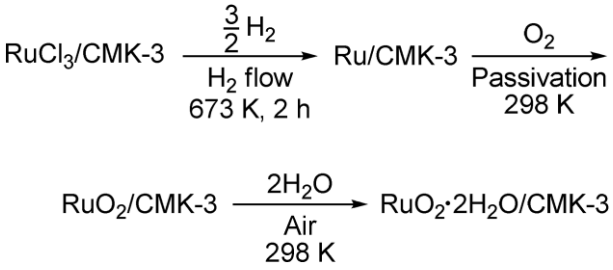

Scheme 3. Formation pathway of the oxidized Ru species on CMK-3 during the catalyst preparation.